Journal of Solid State Chemistry 182 (2009) 1115–1120

Contents lists available at ScienceDirect

Journal of Solid State Chemistry

journal homepage: www.elsevier.com/locate/jssc

Crystal structure and thermal expansion of the low- and high-temperature forms of $BaM^{IV}(PO_4)_2$ compounds ($M = $ Ti, Zr, Hf and Sn)

D. Bregiroux [a,*], K. Popa [b], R. Jardin [c], P.E. Raison [c], G. Wallez [a], M. Quarton [a], M. Brunelli [d], C. Ferrero [d], R. Caciuffo [c]

[a] UPMC Univ. Paris 06, CNRS-UMR 7574, ENSCP-ParisTech, Laboratoire de Chimie de la Matière Condensée de Paris, 11 rue Pierre et Marie Curie, 75231 Paris Cedex 05, France
[b] "Al.I. Cuza" University, Department of Chemistry, 11-Carol I Blvd., 700506 Iasi, Romania
[c] European Commission, Joint Research Centre, Institute for Transuranium Elements, P.O. Box 2340, 76125 Karlsruhe, Germany
[d] ESRF, 6 rue Jules Horowitz, BP 220-38043 Grenoble Cedex, France

ARTICLE INFO

Article history:
Received 9 December 2008
Received in revised form
12 January 2009
Accepted 6 February 2009
Available online 21 February 2009

Keywords:
Thermal expansion
Crystal structure
Phosphate-based materials

ABSTRACT

The crystal structure of β-$BaZr(PO_4)_2$, archetype of the high-temperature forms of $BaM(PO_4)_2$ phosphates (with $M = $ Ti, Zr, Hf and Sn), has been solved *ab initio* by Rietveld analysis from synchrotron X-ray powder diffraction data. The phase transition appears as a topotactic modification of the monoclinic (S.G. $C2/m$) lamellar α-structure into a trigonal one (S.G. $P\bar{3}m1$) through a simple mechanism involving the unfolding of the $[Zr(PO_4)_2]_n^{2-}$ layers. The thermal expansion is very anisotropic (e.g., $-4.1 < \alpha_i < 34.0 \times 10^{-6}\,K^{-1}$ in the case of α-$BaZr(PO_4)_2$) and quite different in the two forms, as a consequence of symmetry. It stems from a complex combination of several mechanisms, involving bridging oxygen rocking in M–O–P linkages, and "bond thermal expansion".

1. Introduction

The double phosphates $BaM^{IV}(PO_4)_2$ have several potential applications, such as immobilization of tetravalent actinides [1,2], UV-emitting X-ray phosphors [3], catalysts and ion conductors [4]. Therefore, the investigation of their crystal chemistry becomes of prime importance. Previous works highlighted that the crystal structure depends on the nature the cation M^{IV}. For $M = $ Ti, Zr, Hf, Ge, Sn and Mo, the $BaM^{IV}(PO_4)_2$ compounds exhibit a crystal structure in the $C2/m$ space group at room temperature (structure called α-$BaM^{IV}(PO_4)_2$, Fig. 1) [5–8]. This monoclinic structure is similar to that of the yavapaiite $KFe(SO_4)_2$, which consists of layers running parallel to the (a,b) plane built up of corner-connected MO_6 octahedra and PO_4 tetrahedra. The fourth vertex of each tetrahedron points into the interlayer where the alkaline Earth Ba takes place, in a ten-fold oxygen environment. It has been reported recently that $BaM^{IV}(PO_4)_2$ undergoes a reversible phase transition during heating for $M = $ Zr and Hf, at 733 and 791 K, respectively [1,4,9,10]. If, for both compounds, the β structure seems to belong to the hexagonal or trigonal system, the space group and consequently the crystal structure, called β-$BaM^{IV}(PO_4)_2$, remained undetermined. Based on Raman spectroscopic studies, Popa and Geisler showed that the high-temperature structure of $BaM^{IV}(PO_4)_2$ compounds (with $M = $ Zr and Hf) is only consistent with the space groups $P\bar{3}1m$, $P\bar{3}m1$ or $R\bar{3}m$ [9,10]. In the frame of the researches carried out on the specific conditioning of transuranic elements, Montel et al. obtained $BaTh(PO_4)_2$ in the monazite structure $P2_1/n$ only at 2.5 kbar [11]. At room temperature, the structure remains undetermined [12] even if, recently, Popa inferred that it should be similar to that of $RbEu(SO_4)_2$ (S.G. $C2/c$) for $M = $ Th and Np. Colani mentioned the existence of $BaU(PO_4)_2$ [13]. Nevertheless, this result is very doubtful (see [7] and references therein for further discussion).

Insofar as the potential applications of this family of compounds involve a wide spectrum of cations (transition, lanthanides, transuranic and p-block elements), it is necessary to establish the relationship between the cation and the resulting structure, including its thermal behavior. The objective of the present work is to determine the structure of β-$BaM^{IV}(PO_4)_2$ (with $M = $ Zr and Hf). This was achieved from Rietveld analysis [14] of synchrotron X-ray diffraction data. The lattice thermal expansion is derived from the evolution of the crystal parameters during heating (with $M = $ Ti, Zr, Hf and Sn), and the mechanism of the phase transition is described.

2. Experimental

The $BaM^{IV}(PO_4)_2$ compounds were obtained from a conventional solid state route. Based on the previous work of Popa et al.

* Corresponding author. Fax: +33 146347489.
E-mail address: damien-bregiroux@enscp.fr (D. Bregiroux).

0022-4596/$ - see front matter © 2009 Elsevier Inc. All rights reserved.
doi:10.1016/j.jssc.2009.02.012

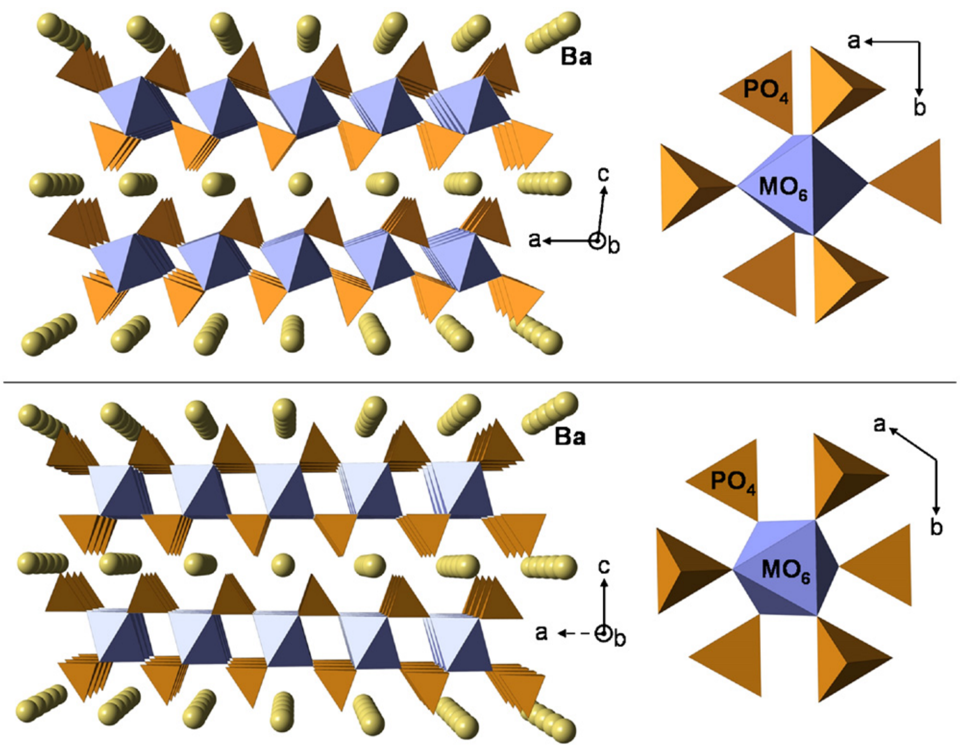

Fig. 1. Crystal structures of α-Ba$M^{IV}(PO_4)_2$ (upper panel, from [6]) and β-Ba$M^{IV}(PO_4)_2$ (lower panel, this work) viewed along the *b*-axis and the *c*-axis.

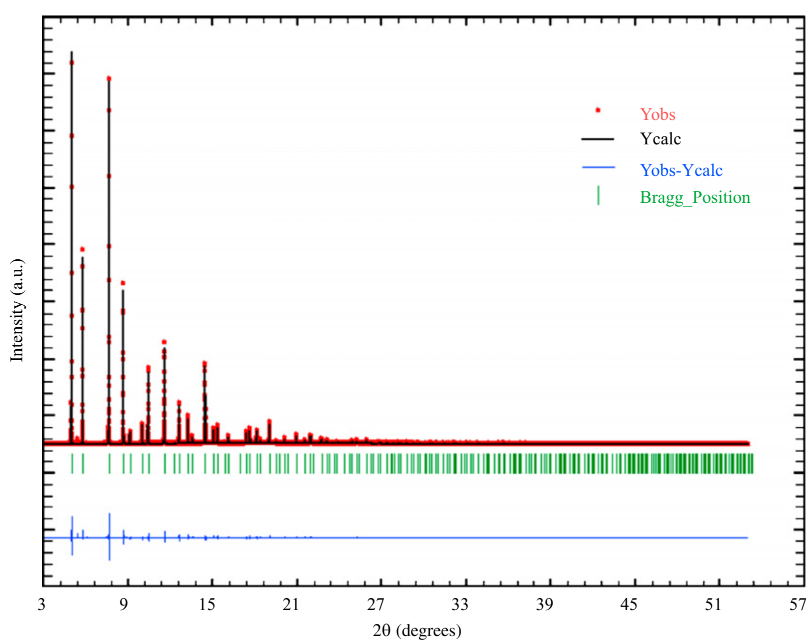

Fig. 2. Rietveld refinement plot of the β-$BaZr(PO_4)_2$ structure at 873 K: observed Y_{obs} (dots), calculated Y_{calc} (solid), angular positions of possible Bragg reflections (bars) and difference curve $Y_{obs}-Y_{calc}$ (lower plot).

[1], a mixture of $BaCO_3$ (Prolabo, 99.5%), MO_2 (Aldrich, 99.9%) and $NH_4H_2PO_4$ (Aldrich, 99.99%) were ground and fired slowly in air up to 1473 K for 100 h in a platinum crucible. The resulting compounds were mainly single-phased. The determination of the β-Ba$M^{IV}(PO_4)_2$ structure was carried out on $BaZr(PO_4)_2$ from high resolution X-ray powder diffraction data collected at the ID31 beam line [15] at the ESRF (Grenoble, France). The sample was loaded into a 0.8 mm diameter glass capillary, mounted on the axis of the diffractometer and spun during measurements. The sample was heated to $T = 873$ K using a hot air blower mounted vertically normal to the capillary rotation axis. The experimental powder diffraction pattern was indexed by the dichotomy method using DICVOL04 software [16]. The crystal structure was then determined *ab initio* from the diffracted intensities extracted using the Fullprof suite of programs in the profile matching mode (Le Bail method) [17]. Patterson method and Fourier-differences were then applied using GFOURIER software [18]. Fig. 2 shows the final Rietveld refinement of the β-$BaZr(PO_4)_2$ structure at 873 K. The background was fitted by linear interpolation between 16 points.

The mechanism of thermal expansion was investigated on $BaM(PO_4)_2$ (with $M =$ Ti, Zr, Hf and Sn) by high-temperature X-ray diffraction (HTXRD) analyses performed on a Philips PW1050/25 17 cm vertical goniometer with a Ni-filtered copper anticathode (40 kV, 20 mA), fitted with a Pt-Rh(40%) heating sample holder. Patterns were recorded up to 1000 °C in the $8^\circ \leqslant 2\theta \leqslant 80^\circ$ range, 2θ step 0.02°, with a counting time of 24 s/step.

The temperature of the $\alpha-\beta$ phase transition was determined in air by differential thermal analysis (Setaram TG 92-16, Pt crucibles) at a heating rate of 5 K min^{-1}.

3. Results

3.1. High-temperature structure of $BaZr(PO_4)_2$

The powder pattern indexing confirms that the structure belongs to the hexagonal system. The unit cell parameters were found to be $a = 5.2145(4)$ Å and $c = 7.8165(4)$ Å. A calculated density of 3.77 g cm^{-3} for a supposed $Z = 1$ number of formular group per cell, is consistent with that of the low temperature α-form (calculated density of 3.88 g cm^{-3} [1]). They were used as starting parameters for the structure refinement. Heavy atoms (i.e. Ba and Zr) coordinates were found by the Patterson method [19] using the trigonal space group with the lowest symmetry, i.e. $P3$. Ba and Zr atoms are located along the three-fold axis ($x = 0$, $y = 0$), and appear approximately $\frac{1}{2}c$ apart ($\Delta z = 0.4978(8)$). The two phosphorus atoms were found by the Fourier-difference method on the ternary axis at the coordinates $(\frac{1}{3}, \frac{2}{3}, z)$ and $(\frac{2}{3}, \frac{1}{3}, z')$. The apical oxygen atoms are located along the same ternary axes. The other oxygen atoms, equivalent by the ternary symmetry, are found to be separated by less than 0.05 Å from the [110] and equivalent planes, suggesting the existence of vertical mirrors. Moreover, taking Ba as the cell origin, it appears that the coordinate of the two phosphorus atoms along c (z and z') are opposite, evidencing their equivalence through a [110] binary axis. Thus, the symmetry and chemical formula (with $Z = 1$) appear fully consistent with the $P\overline{3}m1$ space group. In that case, the refinement leads to oxygen atoms located along [x, $2x$, z], i.e. on a mirror. Taking either space group $P3$ or $P\overline{3}m1$, the atomic coordinates are almost unchanged ($\delta_{max} = 0.05$ Å) as well as the reliability factor R_{Bragg} (i.e. 0.029). One can conclude that the high-temperature form of $BaZr(PO_4)_2$ crystallizes in the $P\overline{3}m1$ space group. Data collection, refinement conditions and crystallographic data are reported in Table 1, final atomic coordinates in Table 2 and cation–anion distances in Table 3.

The crystal structure of β-$BaM(PO_4)_2$ is very similar to that of α-$BaM(PO_4)_2$ (Fig. 1) and can be considered as full isotypic with $KAl(MoO_4)_2$ [21,22]. It consists in (001) layers made of corner-sharing PO_4 tetrahedra and MO_6 octahedra. The main difference with the α form is that faces of polyhedra lie parallel to the ab plane, yielding the highest possible symmetry of the layers. Moreover, the Ba atoms are in that case in a twelve-fold environment (Fig. 3). In such a configuration, the BaO_{12} and MO_6 polyhedra are faces-connected, whereas BaO_{10} and MO_6 polyhedra share only edges in the α form. In α and β forms, the PO_4 tetrahedra and the barium polyhedra are edge-connected.

Table 1
Data collection, refinement conditions and crystallographic data for β-$BaZr(PO_4)_2$ at 873 K.

Data collection	
Method	X-ray diffraction
Temperature (K)	873
Apparatus	ID31 beam line, ESRF
Radiation wavelength (Å)	0.39463(2)
Monochromator	Double-crystal Si(111)
Scan limits, step	$3.00 < 2\theta < 53.00^\circ$, continuous scan (raw data rebinned in 0.002 ° step 2θ)
Refinement conditions	
Observed reflections	914
I-dependent parameters	16
R_p	0.061
R_{wp}	0.078
R_{Bragg}	0.029
R_{exp}	0.044
R_F	0.011
χ^2	3.14
Crystallographic data	
System, space group	Trigonal, $P\overline{3}m1$ (n° 164)
Cell parameters	$a = 5.2145(4)$ Å $c = 7.8165(4)$ Å $V = 184.06(12)$ Å^3
Formula weight (g mol^{-1})	418.503
Z, calculated density(g cm^{-3})	1, 3.77

Table 3
Oxygen environments of Ba, Zr and P in β-$BaZr(PO_4)_2$ at 873 K.

Ba–O(1)^{I,II,III,IV,V,VI} (×6)	3.060(7)
Ba–O(2)^{I,II,III,IV,V,VI} (×6)	3.053(4)
Bond valence sum	1.5 (1.8)^a
Zr–O(2)^{I,II,III,VII,VIII,IX} (×6)	2.039(3)
Bond valence sum	4.5 (4.2)^a
P–O(1)^{III}	1.546(5)
P–O(2)^{III,X,XI} (×3)	1.525(3)
Bond valence sum	4.9 (4.7)^a

Symmetry transformations used to generate equivalent atoms: $^{I}-y, -x, z-1/2$; $^{II}x, -x, z-1/2$; $^{III}x, y, z-1/2$; $^{IV}-x, -y, 3/2-z$; $^{V}-x, x, 3/2-z$; $^{VI}y, x, 3/2-z$; $^{VII}-x, -y, 1/2-z$; $^{VIII}y, x, 1/2-z$; $^{IX}-x, x, 1/2-z$; $^{X}1-y, 1-x, z-1/2$; $^{XI}x, 1-x, z-1/2$.
Bond valence sum calculated using Brese formula [20].
[a] In brackets, bond valence sum for α-$BaZr(PO_4)_2$ at room temperature, calculated from [4].

Table 2
Atomic coordinates and displacement factors (×10^4) of β-$BaZr(PO_4)_2$ at 873 K.

Atom	x	y	z	Wyckoff	U_{11}^{a}	U_{22}^{a}	U_{33}^{a}	U_{12}^{a}	U_{13}^{a}	U_{23}^{a}
Ba	0	0	0	1a	3.80(3)	U_{11}	1.11(2)	$-\frac{1}{2}U_{11}$	0	0
Zr	0	0	$\frac{1}{2}$	1b	1.14(3)	U_{11}	0.92(3)	$-\frac{1}{2}U_{11}$	0	0
P	$\frac{1}{3}$	$\frac{2}{3}$	0.7320(3)	2d	1.41(3)	U_{11}	0.92(4)	$-\frac{1}{2}U_{11}$	0	0
O(1)	$\frac{1}{3}$	$\frac{2}{3}$	0.9298(5)	2d	7.35(2)	U_{11}	0.44(9)	$-\frac{1}{2}U_{11}$	0	0
O(2)	0.1745(4)	2x	0.6655(4)	6i	4.02(9)	3.68(8)	1.94(8)	$-\frac{1}{2}U_{11}$	0	−1.38(9)

[a] U_{ij} (Å^2).

3.2. Thermal expansion of $BaM^{IV}(PO_4)_2$ (M = Ti, Zr, Hf and Sn)

The thermal expansion of $BaM^{IV}(PO_4)_2$ was measured for M = Ti, Zr, Hf and Sn. The cell parameters and the temperature of the $\alpha-\beta$ transition are reported in Table 4.

Because of the limited temperature of the HTXRD equipment (approximately 1273 K), the thermal expansion of the high-temperature form of $BaM^{IV}(PO_4)_2$ was measured only for M = Zr and Hf. Fig. 4 illustrates the thermal expansion of the cell edges of the two forms of $BaM^{IV}(PO_4)_2$ in the case of M = Hf. The cell parameters increase linearly, except a, which presents a stronger expansion at high temperature. Nevertheless, all the relative thermal expansion coefficients are calculated by linear fit. The values are reported for all the investigated compounds in Table 5. Note that in the α form, the β angle slowly decreases when heating.

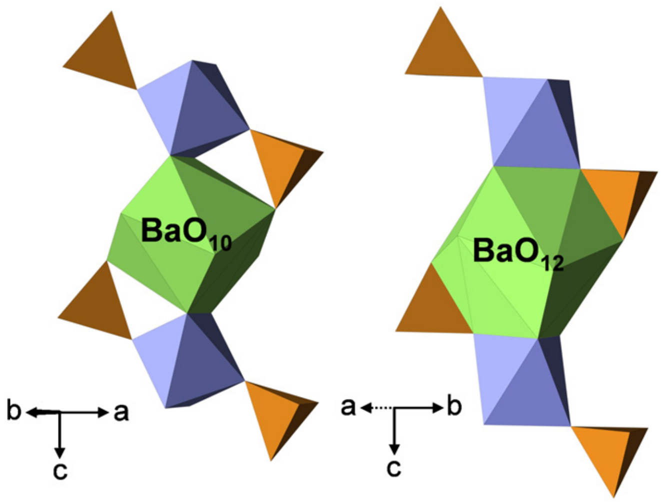

Fig. 3. Barium environment in α-(left) and β-Ba$M(PO_4)_2$ (right): from a ten-(shared edges) to a twelve-fold environment (shared faces).

4. Discussion

4.1. Thermal expansion of the α forms

A strong similarity is pointed out between the α and the β forms of Ba$M(PO_4)_2$. Up to the transition point, the (010) layers of the α form unfold through opposite rotations of the MO_6 and PO_4 polyhedra (Fig. 5, left), thus resulting in a strong thermal expansion, particularly following the a-axis ($\alpha_a = 25–35 \times 10^{-6}\,K^{-1}$).

In contrast, the thermal expansion along b is slightly negative because of the rocking motion of the O(2) oxygen shared by the MO_6 and PO_4 polyhedra. This oxygen oscillates within an ellipsoid oriented roughly perpendicular to the M–O–P axis (Fig. 6). Since the M–O and P–O bonds are strong enough to present negligible thermal expansion, the transverse motion of oxygen pulls the cations closer together [23]. As observed by Wallez et al. for $M_2O(PO_4)_2$ compounds [24,25] and by Taylor for MP_2O_7 compounds [26], a bigger M cation leads to less rigid MO_6 polyhedra, and consequently enhances the rocking motion of the bridging oxygen. However, this tendency is not observed for $BaSn(PO_4)_2$. Indeed, whereas Sn^{+IV} is approximately of the same size as Hf^{+IV} in

Table 4
Transition temperature, space group, density and cell parameters of α- and β-Ba$M(PO_4)_2$ at 293 K (α form) and 873 K (β form).

	$T_{\alpha\rightarrow\beta}$ (K)	S.G.	Z	a (Å)	b (Å)	c (Å)	Angle (deg) if≠90°	V (Å^3)	d_{calc}
α-BaTi(PO$_4$)$_2$	1235	$C2/m$	2	8.2728(3)	5.1903(2)	7.7373(3)	β = 94.18	331.61(1)	3.57
β-BaTi(PO$_4$)$_2$						ND[a]			
α-BaZr(PO$_4$)$_2$	747	$C2/m$	2	8.5603(2)	5.3083(2)	7.8957(2)	β = 93.11	358.26(5)	3.88
β-BaZr(PO$_4$)$_2$		$P\bar{3}m1$	1	5.2145(4)		7.8165(4)	γ = 120	184.06(9)	3.77
α-BaHf(PO$_4$)$_2$	788	$C2/m$	2	8.5509(3)	5.2977(2)	7.8891(3)	β = 93.17	356.82(8)	4.71
β-BaHf(PO$_4$)$_2$		$P\bar{3}m1$	1	5.2054(2)		7.8001(2)	γ = 120	182.96(4)	4.59
α-BaSn(PO$_4$)$_2$	1604	$C2/m$	2	8.2057(2)	5.2396(2)	7.8845(3)	β = 94.54	338.44(2)	4.38
β-BaSn(PO$_4$)$_2$						ND[a]			

[a] ND: not determined.

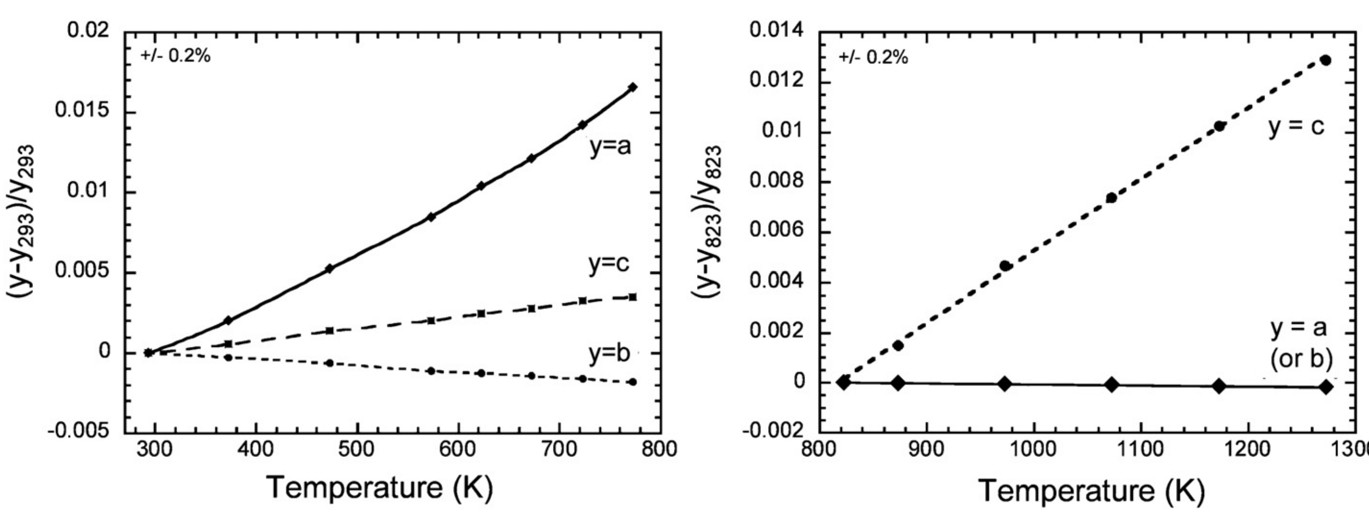

Fig. 4. Relative variation of the cell parameters of α-BaHf(PO$_4$)$_2$ (left) and β-BaHf(PO$_4$)$_2$ (right) with temperature.

Table 5
Relative thermal expansion coefficients ($10^{-6}\,K^{-1}$) for α-and β-Ba$M(PO_4)_2$ obtained by linear fit ($R^2 > 0.99$) over the 293 K–$T_{\alpha\to\beta}$ and the $T_{\alpha\to\beta}$–1273 K range, respectively.

	α-Ba$M(PO_4)_2$					β-Ba$M(PO_4)_2$			
	α_a	α_b	α_c	α_V	$\alpha_1=\frac{1}{3}\alpha_V$	$\alpha_a=\alpha_b$	α_c	α_V	$\alpha_1=\frac{1}{3}\alpha_V$
Ti	26.5	−1.2	13.3	40.5	13.5	ND[a]			
Zr	34.0	−4.1	7.3	38.3	12.8	−1.3	30.7	28.1	9.4
Hf	34.2	−3.8	7.4	39.3	13.1	−0.4	28.7	27.9	9.3
Sn	25.4	−0.9	13.3	40.5	13.5	ND[a]			

[a] ND: not determined.

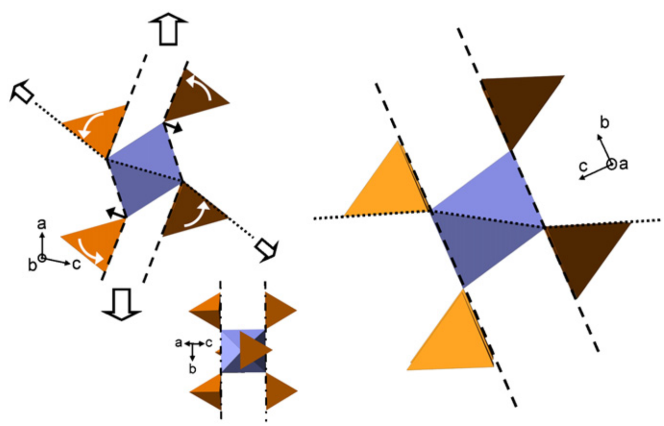

Fig. 5. The (010) $[M(PO_4)_2]_n^{2-}$ layers of α-Ba$M(PO_4)_2$ (left) unfold to give the expanded β array (right).

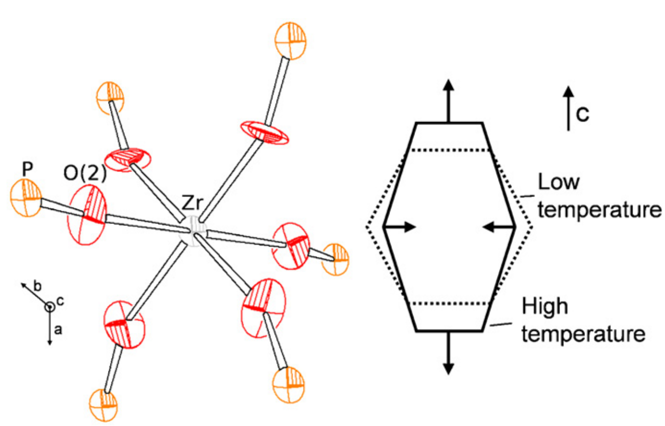

Fig. 6. ORTEP view [27] of the displacement ellipsoids of bridging oxygen atoms between MO_6 and PO_4 polyhedra (left), and schematic anisotropic thermal expansion of BaO_{12} polyhedra (right) in β-Ba$M(PO_4)_2$.

six-fold coordination, it presents also a much higher electronegativity, responsible for stronger and more directed Sn–O bonds. Regarding its thermal expansion, $BaSn(PO_4)_2$ can thus be considered as similar to $BaTi(PO_4)_2$, despite the smaller size of Ti^{IV}. This nature of chemical bonds is in agreement with the high transition temperatures of $BaTi(PO_4)_2$ and $BaSn(PO_4)_2$ in comparison with that of $BaZr(PO_4)_2$ and $BaHf(PO_4)_2$.

4.2. Thermal expansion of the β forms

An important increase of thermal expansion of the interlayers is observed above the phase transition. This difference stems from several phenomena: (i) In the room temperature form, the barium and zirconium polyhedra share edges, whereas they are face-connected in the high-temperature form. The screen effect of oxygen atoms is consequently lower in the high-temperature form whereas the cations Ba^{II} and M^{IV} are closer, resulting in strong repulsions; (ii) the unfolding phenomenon that prevailed in the α form does not occur above the transition temperature; therefore, the thermal expansion of the $[Zr(PO_4)_2]^{2-}$ slabs is ruled by the polyhedra rocking, leading to a near-zero expansion along the *a* and *b* axes; (iii) obviously, the dramatic expansion following the *c*-axis comes from the layers of barium atoms, loosely bonded to the $[Zr(PO_4)_2]^{2-}$ blocks. This expansion is enhanced by two structural features:

- the coordination number of Ba has increased from 10 to 12 in the β form, making the bonds weaker and increasing their expansion rate,
- the expansion of the (001) faces of the BaO_{12} polyhedron is blocked by the invariance of the *a* and *b* parameters, thus compelling the polyhedron to expand strongly following the *c*-axis. Fig. 6 (right) illustrates the well-known phenomenon described by Sleight as "bond thermal expansion" [23]: the stretching of the polyhedron following *c* is mechanically balanced by its contraction in the (001) plan. This is the reason why the expansion of the Ba–O bonds, despite strong, do not increase the $\alpha_{a,b}$ coefficient.

The thermal expansion mechanism described above appears in good agreement with the low bond valence sum calculated for barium at 873 K (Table 3). The apparent low valence of Ba^{II} can be simply explained by the fact that Brese's parameters for bond valence calculation usually apply at room temperature, not at 873 K. Thus, the valence is even lower than the Ba–O bond is long. The increase of the bond valence of Zr is a consequence of the bridging oxygen rocking motion which makes its mean position appear closer than its actual one. Consequently, the Zr–O distance is determined from the mean position of the oxygen, i.e. with a configuration of P–O–*M* with an angle close to 180°, leading to an underestimated value.

5. Conclusion

The crystal structures of the α and β forms of Ba$M(PO_4)_2$, pertaining to M = Ti, Zr, Hf and Sn and their thermal behavior are now established, supplementing the crystallographic data on $A^{II}B^{IV}(PO_4)_2$ type compounds. The α–β transition appears to be displacive and is accompanied by an increase in volume of less than 0.5%. This volume change should not affect the integrity of the material when used as sintered pellets.

Although the thermal evolution of the crystal structure follows a quiet simple mechanism which consists in the unfolding of the $[Zr(PO_4)_2]_n^{2-}$ layers, this leads to a complex thermal expansion mechanism involving various phenomena such as bridging oxygen rocking motion in *M*–O–P linkage, "bond thermal expansion"..., resulting in a strong thermal expansion anisotropy, with thermal expansion coefficients in the range −4.1 to $34.2\times10^{-6}\,K^{-1}$. For the high-temperature form of Ba$M(PO_4)_2$, one can consider that the crystal structure only expands along the *c*-axis.

Acknowledgments

We thank the ESRF (Grenoble, France) for provision of beam time on the high-resolution powder diffraction beam line ID31.

Appendix A. Supplementary material

Supplementary data associated with this article can be found in the online version at 10.1016/j.jssc.2009.02.012.

References

[1] K. Popa, R.J.M. Konings, P. Boulet, D. Bouëxière, A.F. Popa, Thermochim. Acta 436 (2005) 51–55.
[2] K. Popa, H. Leiste, T. Wiss, R.J.M. Konings, J. Radioanal. Nucl. Chem. 273 (3) (2007) 563–567.
[3] C.R. Miao, C.C. Torardi, J. Solid State Chem. 155 (2000) 229–232.
[4] K. Fukuda, A. Moriyama, T. Iwata, J. Solid State Chem. 178 (2005) 2144–2151.
[5] R. Masse, A. Durif, C.R. Acad. Sc. Paris 274C (1972) 1692–1695.
[6] M.T. Paques-Ledent, J. Inorg. Nucl. Chem. 39 (1977) 11–17.
[7] K. Popa, D. Bregiroux, R.J.M. Konings, T. Gouder, A.F. Popa, T. Geisler, P.E. Raison, J. Solid State Chem. 180 (2007) 2346–2355.
[8] A. Leclaire, M.M. Borel, J. Chardon, B. Raveau, J. Solid State Chem. 116 (1995) 364–368.
[9] K. Popa, R.J.M. Konings, O. Beneš, T. Geisler, A.F. Popa, Thermochim. Acta 451 (2006) 1–4.
[10] T. Geisler, K. Popa, R.J.M. Konings, A.F. Popa, J. Solid State Chem. 179 (2006) 1490–1496.
[11] J.-M. Montel, J.-L. Devidal, D. Avignant, Chem. Geol. 191 (2002) 89–104.
[12] V. Brandel, N. Dacheux, J. Rousselle. M. Genet, C.R. Chim. 5 (2002) 599–606.
[13] M.A. Colani, C.R. Chim. (1909) 59.
[14] H.M. Rietveld, Acta Crystallogr. 22 (1967) 151–152.
[15] A.N. Fitch, J. Res. Natl. Inst. Stand. Technol. 109 (2004) 133–135.
[16] A. Boultif, D. Louër, J. Appl. Cryst. 37 (2004) 724–731.
[17] J. Rodriguez-Carvajal, FullProf.2k: Rietveld, Profile Matching and Integrated Intensity Refinement of X-ray and Neutron Data, vol. 1.9c, Laboratoire Léon Brillouin, CEA, Saclay, France, 2001.
[18] J. Gonzalez-Platas, J. Rodriguez-Carvajal, GFOURIER: Fourier Maps, Calculation Program, vol. 3.20, Universidad de La Laguna/Laboratoire Léon Brillouin, CEA, Tenerife, Spain/Saclay, France, 2003.
[19] M.G. Rossmann, E. Arnold, second ed., International Tables for Crystallography, vol. B 2–3, Springer, New York, 2006, pp. 235–263.
[20] N.E. Brese, M. O'Keeffe, Acta Crystallogr. B47 (1991) 192–197.
[21] R.F. Klevtsova, P.V. Klevtsov, Kristallografiya 15 (1970) 953–959.
[22] S. Oyetola, A. Verbaere, Y. Piffard, M. Tournoux, Eur. J. Solid State Inorg. Chem. 25 (1988) 259–278.
[23] A.W. Sleight, Inorg. Chem. 37 (1998) 2854–2860.
[24] G. Wallez, S. Launay, J.-P. Souron, M. Quarton, E. Suard, Chem. Mater. 15 (2003) 3793–3797.
[25] G. Wallez, S. Launay, M. Quarton, N. Dacheux, J.-L. Soubeyroux, J. Solid State Chem. 177 (2004) 3575–3580.
[26] D. Taylor, Br. Ceram. Trans. J. 87 (1988) 39–45.
[27] L.J. Farrugia, J. Appl. Cryst. 30 (1997) 565.